Monthly Notices
of the
ROYAL ASTRONOMICAL SOCIETY

Mon. Not. R. Astron. Soc. **424,** 333–347 (2012) doi:10.1111/j.1365-2966.2012.21201.x

The chemical diversity of exo-terrestrial planetary debris around white dwarfs

B. T. Gänsicke,[1]⋆ D. Koester,[2] J. Farihi,[3] J. Girven,[1] S. G. Parsons[1] and E. Breedt[1]

[1]*Department of Physics, University of Warwick, Coventry CV4 7AL*
[2]*Institut für Theoretische Physik und Astrophysik, University of Kiel, 24098 Kiel, Germany*
[3]*Department of Physics Astronomy, University of Leicester, Leicester LE1 7RH*

Accepted 2012 April 26. Received 2012 April 26; in original form 2012 March 23

ABSTRACT

We present *Hubble Space Telescope* (*HST*) ultraviolet spectroscopy of the white dwarfs PG 0843+516, PG 1015+161, SDSS 1228+1040, and GALEX 1931+0117, which accrete circumstellar planetary debris formed from the destruction of asteroids. Combined with optical data, a minimum of five and a maximum of 11 different metals are detected in their photospheres. With metal sinking time-scales of only a few days, these stars are in accretion/diffusion equilibrium, and the photospheric abundances closely reflect those of the circumstellar material. We find C/Si ratios that are consistent with that of the bulk Earth, corroborating the rocky nature of the debris. Their C/O values are also very similar to those of bulk Earth, implying that the planetary debris is dominated by Mg and Fe silicates. The abundances found for the debris at the four white dwarfs show substantial diversity, comparable at least to that seen across different meteorite classes in the Solar system. PG 0843+516 exhibits significant overabundances of Fe and Ni, as well as of S and Cr, which suggests the accretion of material that has undergone melting, and possibly differentiation. PG 1015+161 stands out by having the lowest Si abundance relative to all other detected elements. The Al/Ca ratio determined for the planetary debris around different white dwarfs is remarkably similar. This is analogous to the nearly constant abundance ratio of these two refractory lithophile elements found among most bodies in the Solar system.

Based on the detection of all major elements of the circumstellar debris, we calculate accretion rates of $\simeq 1.7 \times 10^8$ to $\simeq 1.5 \times 10^9$ g s^{-1}. Finally, we detect additional circumstellar absorption in the Si IV 1394, 1403 Å doublet in PG 0843+516 and SDSS 1228+1040, reminiscent to similar high-ionization lines seen in the *HST* spectra of white dwarfs in cataclysmic variables. We suspect that these lines originate in hot gas close to the white dwarf, well within the sublimation radius.

Key words: stars: individual: PG 0843+516 – stars: individual: PG 1015+161 – stars: individual: SDSS J122859.93+104032.9 – stars: individual: GALEX J193156.8+011745 – planetary systems – white dwarfs.

1 INTRODUCTION

Most of our current insight into the interior structure of exoplanets is derived from the bulk density of transiting planets (e.g. Valencia et al. 2010), and transit spectroscopy provides some information on the chemical composition of their atmospheres (e.g. Grillmair et al. 2008). More detailed investigations of the chemistry of exo-planetary systems around main-sequence host stars are beyond the reach of present observational instrumentation. However, Zuckerman et al. (2007) demonstrated in a pioneering paper that the photospheric abundances of the polluted white dwarf GD 362 can be used to infer the bulk abundances of the planetary debris material detected around this star, and showed that the composition of this material is broadly comparable to that of the Earth–Moon system.

The strong surface gravity of white dwarfs implies that metals will sink out of the photosphere on time-scales that are orders of magnitude shorter than their cooling ages, and therefore white dwarfs are expected to have either pure hydrogen or helium atmospheres (Fontaine & Michaud 1979). Exceptions to this rule are only hot ($T_{\rm eff} \gtrsim 25\,000$ K) white dwarfs where radiative levitation can support some heavy elements in the photosphere (e.g. Chayer, Fontaine & Wesemael 1995), and cool ($T_{\rm eff} \lesssim 10\,000$ K) white dwarfs where

⋆E-mail: boris.gaensicke@warwick.ac.uk

convection may dredge up core material (Koester, Weidemann & Zeidler 1982; Fontaine et al. 1984). Yet white dwarfs with metal-contaminated atmospheres have been known for nearly a century (van Maanen 1917), and accretion from the interstellar medium (e.g. Koester 1976; Wesemael 1979; Dupuis, Fontaine & Wesemael 1993) has been the most widely accepted scenario, despite a number of fundamental problems (e.g. Aannestad et al. 1993; Friedrich, Jordan & Koester 2004; Farihi et al. 2010a). However, the rapidly growing number of white dwarfs that are accreting from circumstellar discs (e.g. Becklin et al. 2005; Kilic et al. 2005; Gänsicke et al. 2006; von Hippel et al. 2007; Farihi, Zuckerman & Becklin 2008; Vennes, Kawka & Németh 2010; Dufour et al. 2012) unambiguously demonstrates that debris from the tidal disruption of main-belt analogue asteroids or minor planets (Graham et al. 1990; Jura 2003), or Kuiper-belt like objects (Bonsor, Mustill & Wyatt 2011), likely perturbed by unseen planets (Debes & Sigurdsson 2002; Debes, Walsh & Stark 2012), is the most likely origin of photospheric metals in many, if not most polluted white dwarfs.

Because of the need for high-resolution, high-quality spectroscopy, detailed abundance studies have so far been limited to a handful of white dwarfs (Klein et al. 2010, 2011; Vennes, Kawka & Németh 2011b; Melis et al. 2011; Zuckerman et al. 2011; Dufour et al. 2012; Jura et al. 2012). For a given abundance and white dwarf temperature, metal lines are stronger in a helium-dominated (DB) atmosphere than in a hydrogen-dominated (DA) atmosphere, as the opacity of helium is much lower than that of hydrogen. Therefore, the small sample of well-studied metal polluted white dwarfs is heavily biased towards DB white dwarfs, which have diffusion time-scales of $\sim 10^5$–10^6 yr. These long diffusion time-scales introduce a significant caveat in the interpretation, as the abundances of the circumstellar debris may substantially differ from those in the white dwarf photosphere if the accretion rate varies on shorter time-scales (Koester 2009). While the lifetimes of the debris discs are subject to large uncertainties, there are theoretical (Rafikov 2011; Metzger, Rafikov & Bochkarev 2012) and observational (Farihi et al. 2012a; Girven et al. 2012) arguments that suggest that the accretion rates on to the white dwarfs may vary significantly over periods that are short compared to the diffusion time-scales. In fact, some of the most heavily polluted white dwarfs have no infrared excess (Farihi, Jura & Zuckerman 2009; Klein et al. 2011), and may have accreted all the circumstellar debris a few diffusion time-scales ago (Farihi et al. 2009; Girven et al. 2012).

We are currently carrying out an ultraviolet spectroscopic survey of young DA white dwarfs that have cooling ages of 20 to 200 Myr, metal sinking time-scales of a few days, and are hence guaranteed to be in accretion–diffusion equilibrium. The aim of this survey is to determine the fraction of white dwarfs that are presently accreting planetary debris, and to measure accurate abundances for a subset. Here we present the analysis of four heavily polluted white dwarfs that are known to also host planetary debris discs.

2 OBSERVATIONS

The targets for our ongoing far-ultraviolet spectroscopic survey of young and correspondingly warm ($17\,000\,\mathrm{K} < T_{\rm eff} < 25\,000\,\mathrm{K}$) DA white dwarfs were drawn from the compilations of Liebert, Bergeron & Holberg (2005) and Koester et al. (2009), supplemented with a few recent discoveries (e.g. Gänsicke et al. 2006; Vennes et al. 2010). Our sample also includes a small number of post-common envelope binaries (PCEBs) in which the white dwarf accretes from the wind of the M-dwarf companion. These systems were selected from Schreiber & Gänsicke (2003) and Farihi, Hoard & Wachter (2010b) with the same cut on white dwarf temperature and cooling age. Under the assumption that the M-dwarfs have a solar-like composition, the white dwarfs in PCEBs serve as 'abundance standards' for our abundances analyses and diffusion calculations.

2.1 *HST*/COS spectroscopy

PG 0843+516, PG 1015+161 and GALEX J193156.8+011745 (henceforth GALEX 1931+0117) were observed as part of our snapshot survey, with exposure times of 1420 s, 1424 s and 800 s, respectively. We used the G130M grating with a central wavelength of 1291 Å, which covers the wavelength range 1130–1435 Å, with a gap at 1278–1288 Å due to the space between the two detector segments. To mitigate the fixed pattern noise that is affecting the Cosmic Origin Spectrograph (COS) far-ultraviolet detector, we split the exposure time equally between two FP-POS positions (1 and 4, the limited duration of the snapshot visits did not allow us to use the full set of four different FP-POS positions).

We also report COS observations of three PCEBs observed within this snapshot survey, that will be used as 'abundances standards': GD 448 (HR Cam; Maxted et al. 1998), GD 245 (MS Peg; Schmidt et al. 1995), and PG 2257+162 (KUV 22573+1613; Wachter et al. 2003), with exposure times of 900 s, 600 s and 1070 s, respectively.

SDSS J122859.93+104032.9 (henceforth SDSS 1228+1040) was observed in Cycle 17 as part of a regular Guest Observer programme. We obtained two sets of spectroscopy with the G130M grating with central wavelengths of 1291 and 1327 Å, and both observations were again split among two FP-POS positions (1 and 4). In addition, we obtained G160M spectroscopy with central wavelengths of 1577 Å and 1623 Å. The total exposure time of the G130M and G160M observations was 2821 s and 4899 s, respectively, seamlessly covering the wavelength range 1130–1795 Å.

The data retrieved from the *Hubble Space Telescope* (*HST*) archive were processed and calibrated with CALCOS 2.15.6. The COS spectra of the four white dwarfs shown in Fig. 1 reveal the broad Lyα profile typical of DA white dwarfs, plus a multitude of narrow absorption lines from a range of metals. The peak signal-to-noise ratio (S/N) of the COS spectra is reached in a line-free region near 1320 Å, and ranges from $\simeq$25 for PG 0843+516 and PG 1015+161 to $\simeq$40 for SDSS 1228+1040 and GALEX 1931+0117. However, these values only include photon count statistics, and do not account for the residual fixed-pattern noise related to the use of only two FP-POS positions. The resolving power of the COS spectra as measured from on-orbit data ranges from $\sim$15 000 at 1150 Å to $\sim$20 000 at 1430 Å.

2.2 Optical observations

The wavelength spanned by our COS observations does not cover any strong line of either Ca (traditionally the most important tracer of metal pollution in white dwarfs, and an important refractory element) or Mg (one of the major constituents of rocky material in the Solar system, including the Earth). Ground-based abundance studies using the Ca II H/K doublet and the Mg II 4482 Å line are already published for GALEX 1931+0117 (Vennes et al. 2010, 2011b; Melis et al. 2011). Two short (10 min) spectra of PG 1015+161 were obtained on the Very Large Telescope (VLT) using the Ultraviolet and Visual Echelle Spectrograph (UVES) as part of the SPY project (Napiwotzki et al. 2001), which Koester et al. (2005) analysed to determine the Ca abundance of PG 1015+161 (Section 4.2). Here we use the same spectra to determine in addition the abundance of Mg.

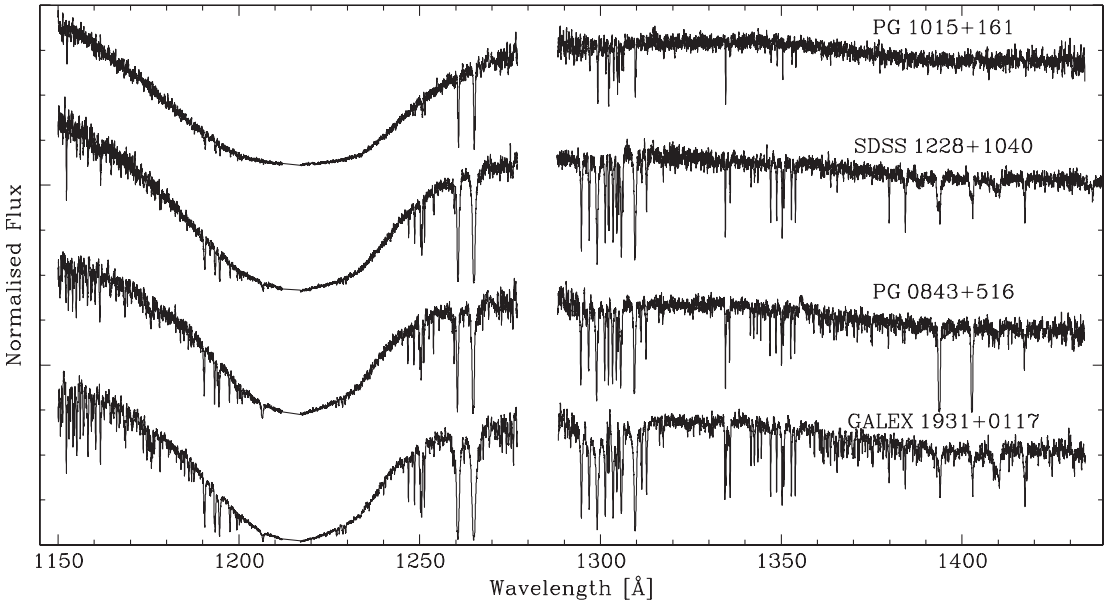

Figure 1. COS/G130M spectra of four white dwarfs known to have circumstellar discs, scaled to a peak flux of unity, offset by 1.4 units, and sorted from top to bottom by increasing metal abundances. For warm white dwarfs with pure hydrogen atmospheres, the broad Lyα line is the only spectral feature in this wavelength range. These four stars accrete from the circumstellar debris, and their spectra are riddled with absorption lines of C, O, Al, Si, P, S, Cr, Fe and Ni. In addition, Mg and Ca can be detected in their optical spectra (Fig. 2).

We observed PG 0843+516 for a total of 2 h on the William Herschel Telescope (WHT) using the dual beam spectrograph ISIS with the R600B grating and a 1*c* slit, covering the Ca and Mg lines at a resolving power of $\simeq$2500 and a S/N of $\approx$90. The data were reduced and calibrated as described in Pyrzas et al. (2012).

We also obtained a total of 9 h VLT/UVES spectroscopy of SDSS 1228+1040 between 2007 and 2009 using the Blue390 and Blue437 setup with a 0.9 arcsec slit, covering both the Ca and Mg features with a resolving power of $\simeq$40 000. The data were reduced in Gasgano using the UVES pipeline. The individual spectra were of relatively low S/N, and we analysed only the error-weighted average spectrum, binned to 0.05 Å, with S/N $\simeq$ 35.

The optical spectra around the Ca II K and Mg II 4482 Å lines are shown in Fig. 2. We note that while most previous studies of metal-polluted white dwarfs have focused on the Ca II H/K lines, their strength for a given abundance decreases strongly with increasing temperature, as Ca II is ionized to Ca III. For temperatures $T_{\rm eff} \simeq$ 20 000–25 000 K, Mg II 4482 Å becomes a more sensitive probe of metal pollution (e.g. Gänsicke, Marsh & Southworth 2007; Farihi et al. 2012b).

3 ATMOSPHERE MODELS

3.1 Effective temperature and surface gravity

All observed *HST*/COS and optical spectra were analysed with theoretical model atmospheres using input physics as described in Koester (2010), and including the Lyman and Balmer line profiles of Tremblay & Bergeron (2009). We used a fine grid of models spanning the range of temperatures and surface gravities found for the four targets by previous studies (Table 1) and determined the best-fitting parameter by minimizing χ^2, using the very good relative flux calibration as an additional constraint. The errors reported in Section 4 are statistical only and do not include systematic effects of observation, reduction or models. More realistic errors can be estimated from a comparison with the other measurements in the literature, which used similar models, but optical spectra. Table 1 suggests a systematic trend for somewhat lower temperatures derived from the ultraviolet data when compared to the values based on optical spectroscopy. A similar trend is seen for DA white dwarfs with $T_{\rm eff} \sim$ 20 000 K in Lajoie & Bergeron (2007), who compared the effective temperatures derived from optical and International Ultraviolet Explorer (IUE) ultraviolet spectroscopy. We carried out a range of test calculations to explore the effect of these systematic uncertainties in $T_{\rm eff}$ and $\log g$ on the derived metal abundances (Section 3.2). The abundances and mass fluxes do not change by more than $\simeq$0.1 dex, which is less than the typical uncertainty of our fits,

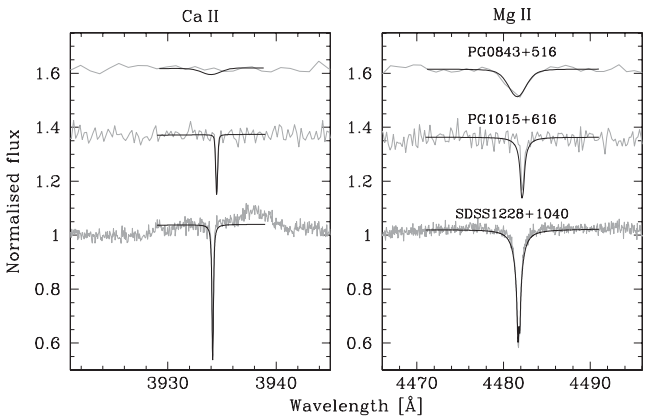

Figure 2. The normalized optical spectra (grey) of PG 0843+516 (WHT), PG 1015+161 (VLT/UVES, binned to 0.2 Å) and SDSS 1228+1040 (VLT/UVES, binned to 0.05 Å), along with the best-fitting models (black). The width of the Mg II line in PG 0843+516 is due to the low resolution of the WHT data. In the spectrum of SDSS 1228+1040, the photospheric absorption of Ca II K is embedded in a double-peaked emission line from the gaseous debris disc, which is, however, so broad that it does not affect the measurement of the Ca abundance.

Table 1. Atmospheric parameters from spectroscopy.

Object	$T_{\rm eff}$ (K)	log g (cgs units)
PG 0843+516 = WD 0843+516		
Optical (Liebert et al. 2005)	23 870 ± 392	7.90 ± 0.05
HST (this paper)	23 095 ± 230	8.17 ± 0.06
PG 1015+161 = WD 1015+161		
Pptical (Liebert et al. 2005)	19 540 ± 305	8.04 ± 0.05
Optical (Koester et al. 2009)	19 948 ± 33	7.925 ± 0.006
HST (this paper)	19 200 ± 180	8.22 ± 0.06
SDSS J122859.93+104032.9 = WD1226+110		
Optical (Eisenstein et al. 2006)	22 125 ± 136	8.22 ± 0.02
Optical (Gänsicke et al. 2007)	22 292 ± 296	8.29 ± 0.05
Optical, our fit to SDSS spectrum	22 410 ± 175	8.12 ± 0.02
HST (this paper)	20 565 ± 82	8.19 ± 0.03
Adopted (this paper, Section 3.1)	20900 ± 900	8.15 ± 0.04
GALEX J193156.8+011745 = WD 1929+012		
Optical (Vennes et al. 2010)	20 890 ± 120	7.90 ± 0.03
Optical (Melis et al. 2011)	23 470 ± 300	7.99 ± 0.05
HST (this paper)	21 200 ± 50	7.91 ± 0.02

and the abundance ratios vary by much less. Hence, the discussion in Sections 5 and 6 is not affected by the systematic uncertainties in $T_{\rm eff}$ and log g.

Finally, to assess the possible effect that the presence of metals has on the effective temperature and surface gravity, we computed a small grid of models for the two most metal-polluted stars (PG 0843+516, GALEX 1931+0117), including metals at the abundances determined in Section 3.2, and re-fitted the *HST*/COS spectra. For both stars, the best-fitting $T_{\rm eff}$ and log g did not change significantly, and we therefore adopted the atmospheric parameters from the pure-hydrogen fits for all four targets.

3.2 Metal abundances

The COS spectra of the four white dwarfs contain a multitude of absorption lines from a range of elements. GALEX 1931+0117 has the richest absorption spectrum, in which we securely identified transitions of nine elements (C, O, Al, Si, P, S, Cr, Fe, Ni), and we included those metals in the abundance analysis of all four targets. We also include in the analysis N, Na, Ti, V, Mn, which have moderately strong transitions in the wavelength range covered by the COS observations, but that were not detected. All metals were fully included in the calculation of the equation of state.

Synthetic spectra were calculated adopting the atmospheric parameters determined in Section 3.1, and including approximately 2500 metal lines. The basic source of atomic line data (wavelengths, excitation energies, transition probabilities log gf, Stark broadening constant Γ_4) was the Vienna Atomic Line Database (VALD), which is described in Piskunov et al. (1995), Ryabchikova et al. (1997) and Kupka et al. (1999, 2000). The ion Si II has a large number of lines in the ultraviolet, and we noted a significant scatter in the abundances derived from different lines. Replacing the log gf values from VALD with those from the National Institute of Standards (NIST) data base, which differ for some lines by up to 0.3 dex, leads to more consistent results. Nevertheless, the situation for this ion is not satisfactory (Section 3.2.2), and we have consulted a number of original sources in the literature (Lanz & Artru 1985; Nahar 1998; Bautista et al. 2009) during the compilation of the most reliable atomic data.

The abundances were varied until a satisfactory fit, as judged by visual inspection, was achieved for each element. We then changed the abundances in several steps of 0.1–0.2 dex, until the fit was clearly worse. The resulting difference was used as a conservative estimate for the abundance error, or for an upper limit if no line was identified. Table 2 lists the lines used in this procedure, although not all lines could be used for all four stars. The best-fitting models to the COS observations are illustrated in Figs 3 and 4, and the metal abundances of the four white dwarfs are given in Table 3 (along with the previous abundance studies that were carried out for GALEX 1931+0117; Melis et al. 2011; Vennes et al. 2011b). Notably, upper limits for N were always larger than solar relative to C. For Na, Ti, V, Mn (and additionally Ca in PG 0843+516 as well as Ca, Al, P, S, Ni in PG 1015+161) the upper limits were larger than solar relative to Si. We have used these (solar) values in the models, but it did not change the atmosphere structure and the results for the detected elements.

Table 2. A list of major line features used for the abundance determinations and upper limits. Because of the different wavelength ranges of the available spectra not all lines could be used for all four stars.

Ion	Vacuum wavelengths (Å)
C II	1334.530,1335.660,1335.708
C III	1174.930,1175.260,1175.590,1175.710,1175.987,1176.370
N I	1199.550,1200.220,1200.710
O I	1152.150,1302.170,1304.860,1306.030
Mg II	1239.925,1240.395,1367.257,1367.708,1369.423, 4482.383,4482.407,4482.583
Al II	1670.787,1719.442,1724.922,1724.982,1760.106,1761.977, 1763.869,1763.952,1765.816
Al III	1379.670,1384.132,1605.766,1611.873
Si II	1190.416,1193.292,1194.500,1197.394,1246.740,1248.426, 1250.091,1250.436,1251.164,1260.422,1264.738,1265.002, 1304.370,1305.592,1309.276,1309.453,1311.256,1346.884, 1348.543,1350.072,1350.516,1350.656,1352.635,1353.721, 1526.707,1533.431,3854.758,3857.112,3863.690,4129.219, 4132.059,5042.430,5057.394,6348.864,6373.132
Si III	1140.546,1141.579,1142.285,1144.309,1144.959,1154.998, 1155.959,1156.782,1158.101,1160.252,1161.579,1206.500, 1206.555,1294.545,1296.726,1298.892,1301.149,1303.323, 1312.591,1341.458,1342.389,1365.253,1417.237
Si IV	1393.775,1402.770
P II	1149.958,1152.818,1153.995,1155.014,1156.970,1159.086, 1249.830,1452.900,1532.533,1535.923,1536.416,1542.304, 1543.133,1543.631
P III	1334.813,1344.326
S II	1250.584,1253.811,1259.519
S III	1194.041,1194.433
Ca II	1169.029, 1169.198,1341.890,3737.965,3934.777
Sc II	1418.773,1418.793
Ti III	1298.633,1298.697,1298.996,1327.603
V III	1148.465,1149.945,1149.945
Cr III	1136.669,1146.342,1247.846,1252.616,1259.018,1261.865, 1263.611
Mn II	1162.015,1188.505,1192.316,1192.330,1197.184,1199.391, 1201.118,1233.956,1254.410
Mn III	1174.809,1177.478,1179.851,1183.308,1183.863,1183.880
Fe II/III	Many weak lines, individually recognisable 1140−1152
Ni II	1317.217,1335.201,1370.123,1381.286,1393.324,1411.065

3.2.1 *Interstellar line absorption and airglow*

In all objects interstellar absorption is visible in the resonance lines of C II, N I, O I, Si II and S II. In SDSS 1228+1040, PG 1015+161 and GALEX 1931+0117 the interstellar absorption lines are shifted

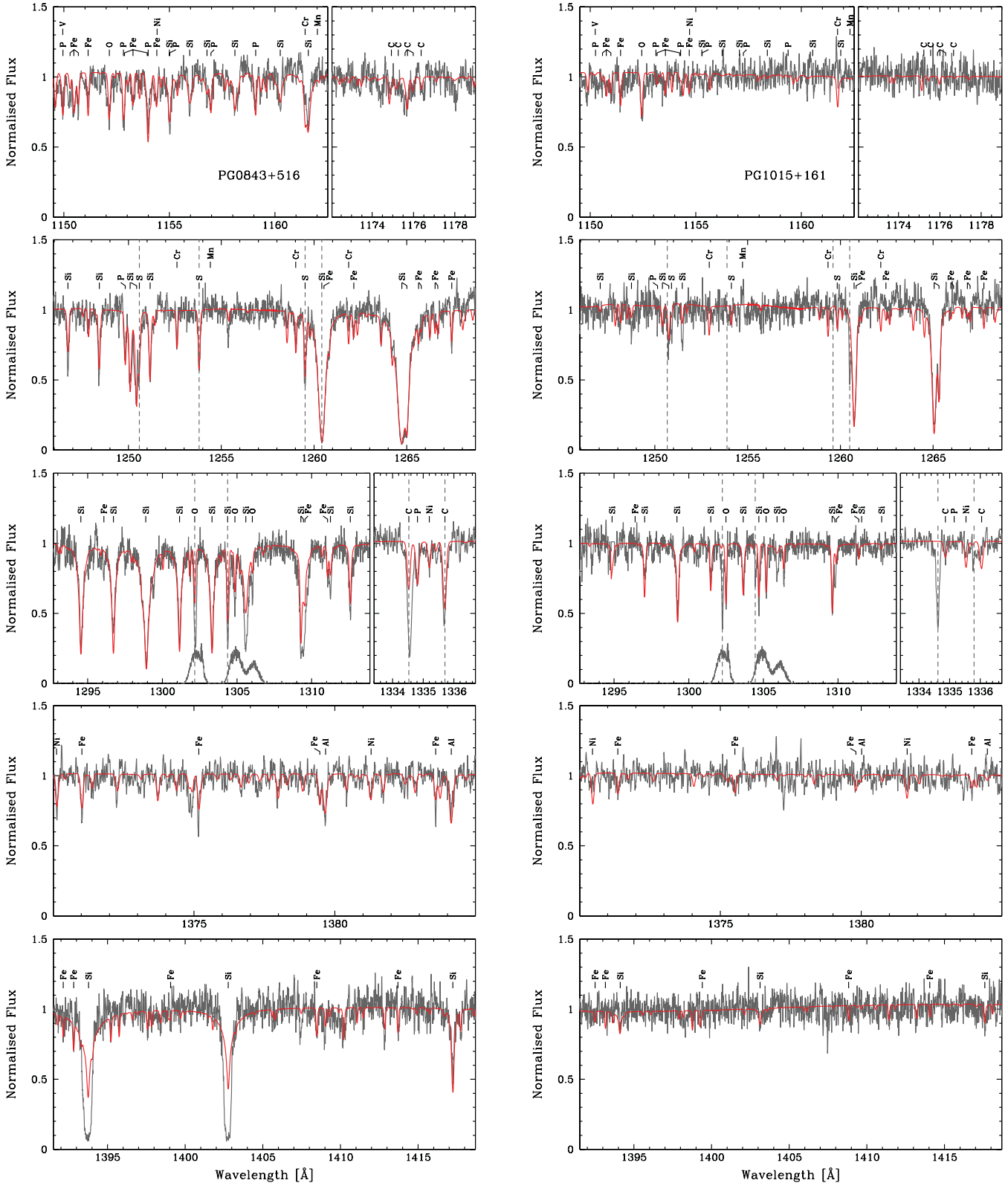

Figure 3. The normalized COS spectra (black) of PG 0843+516 (left) and PG 1015+161 (right), along with our best-fitting models (red). Interstellar absorption features are indicated by vertical grey dashed lines. The interstellar lines in PG 1015+161 are blueshifted with respect to the photospheric features by 57 km s^{-1}; in PG 0843+516 this shift is $\leq$7 km s^{-1}. Airglow of O I can cause some contamination of the 1302–1306 Å region. An illustrative airglow emission spectrum (arbitrarily scaled in flux) is shown. The strong Si IV 1394, 1403 Å doublet seen in the COS spectrum of PG 0843+516 is not of photospheric, but of circumstellar origin (Section 7).

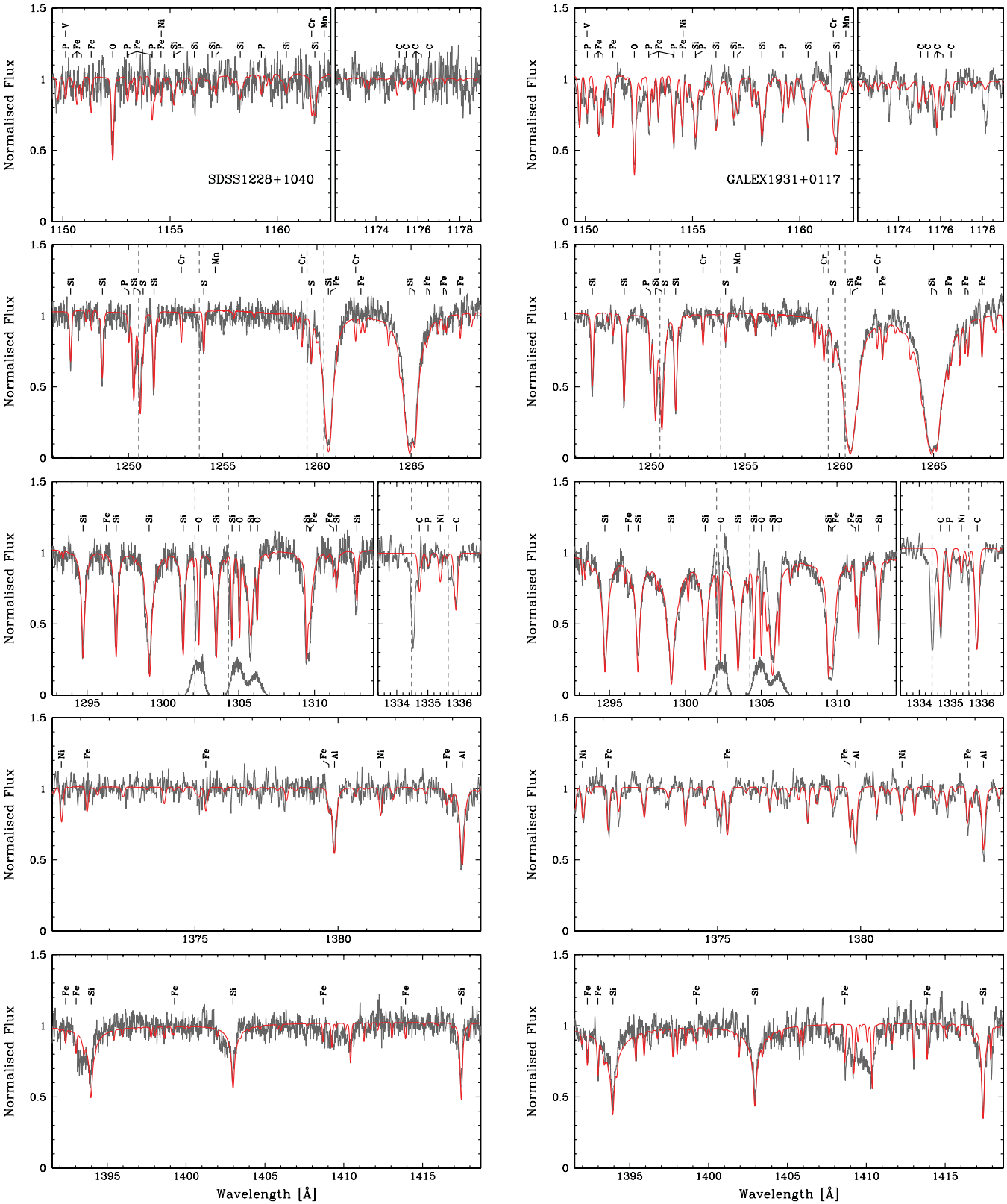

Figure 4. Same as Fig. 3, but for SDSS 1228+1040 (left) and GALEX 1931+0117 (right). The interstellar lines in their spectra are blueshifted with respect to the photospheric features by 36 and 61 km s^{-1}, respectively. The strong absorption band seen near 1410 Å in the COS spectrum of GALEX 1931+0117 is thought to be related to an autoionization line of Si II or to a resonance feature in the photoionization cross-section (Section 3.2.2). The same features are seen, though much weaker, in SDSS 1228+1040. The Si IV 1394, 1403 Å doublet in SDSS 1228+1040 shows additional absorption, blueshifted with respect to the photospheric features, which is of circumstellar origin (Section 7).

Table 3. Element number abundances log [Z/H] and limits determined from the analysis of our *HST*/COS and optical spectra. For Si, we separately report the abundances determined from the optical data alone ('opt'; see Section 3.2.2), and for Ca and Mg, we report both the abundances from a homogenous and a stratified atmosphere ('strat'; see Section 3.2.3), the latter ones are preferred as the strongest lines for both elements are observed in the optical. For GALEX 1931+0117, we also list the results of Vennes et al. (2011b) and Melis et al. (2011).

Element	PG 0843+516	PG 1015+161	SDSS 1228+1040	.....	GALEX 1931+0117	.....
	.....	.....	this paper	.....	Vennes et al.	Melis et al.
C	-7.30 ± 0.30	<-8.00	-7.50 ± 0.20	-6.80 ± 0.30	<-4.15	<-4.85
O	-5.00 ± 0.30	-5.50 ± 0.20	-4.55 ± 0.20	-4.10 ± 0.30	-3.62 ± 0.05	-3.68 ± 0.10
Mg	-4.90 ± 0.20	-5.30 ± 0.20	-5.10 ± 0.20		-4.42 ± 0.06	-4.10 ± 0.10
Mg (strat)	-5.00 ± 0.20	-5.30 ± 0.20	-5.20 ± 0.20			
Al	-6.50 ± 0.20		-5.75 ± 0.20	-6.20 ± 0.20		
Si	-5.20 ± 0.20	-6.40 ± 0.20	-5.20 ± 0.20	-4.75 ± 0.20		
Si (opt)			-4.70 ± 0.20		-4.24 ± 0.07	-4.35 ± 0.11
P	-6.60 ± 0.20		<-7.30	-7.00 ± 0.30		
S	-5.50 ± 0.30		<-6.20	-6.60 ± 0.20		
Ca		-6.30 ± 0.20	-5.70 ± 0.20		-6.11 ± 0.04	-5.83 ± 0.10
Ca (strat)		-6.45 ± 0.20	-5.94 ± 0.20			
Cr	-5.80 ± 0.30	<-5.80	<-6.00	-6.10 ± 0.30		-5.92 ± 0.14
Mn						-6.26 ± 0.15
Fe	-4.60 ± 0.20	-5.50 ± 0.30	-5.20 ± 0.30	-4.50 ± 0.30	-4.43 ± 0.09	-4.10 ± 0.10
Ni	-6.30 ± 0.30		<-6.50	-6.70 ± 0.30		<-5.60

bluewards with respect to the photospheric lines by velocities of $v = 57$, 36 and 61 km s^{-1}, respectively. In PG 0843+516, $|v| < 7$ km s^{-1}, and the interstellar lines are not fully separated from the photospheric features. However, the presence of some interstellar absorption is obvious from the line ratio of C II 1334.5 Å/C II 1335.7 Å (Figs 3 and 4). Because the latter line originates from a level only 0.008 eV above the real ground state, it is equally populated in a stellar photosphere, but not in the interstellar medium, where the blue component is much stronger in spite of a lower transition probability. Nevertheless, the abundances of C, O, Si and S are robust, as a sufficient number of excited transitions are present in the photospheric spectrum (Table 2).

The COS pipeline does not correct for airglow emission. Therefore, the reduced COS spectra can contain geocoronal lines of O I 1302, 1305, 1306 Å whose intensity, and, to a lesser extent, profile shape vary as a function of *HST*'s orbital day/night, and weakly with the Earth-limb angle. Airglow is clearly seen in the spectrum of GALEX 1931+0117 (Fig. 4, right-hand panel), which affects the fit to the photospheric O I and Si II lines in this region. For Si, this is a minor problem as there are many additional lines of Si II–IV. For O, another strong line in the COS spectra is O I 1152 Å.

3.2.2 Silicon

We notice relatively large differences of the silicon abundance determined from optical versus ultraviolet spectra in SDSS 1228+1040 and GALEX 1931+0117; for the latter also the oxygen abundances show this difference. There are at least three possible explanations.

Uncertain atomic data. This is a perennial problem, as there are many, and large, differences in various compilations of atomic data. The O I resonance lines in GALEX 1931+0117 are perturbed by airglow, interstellar absorption and overlapping Si II lines (see above), and the ultraviolet abundance determination rests largely on one excited line at 1152.1 Å. Similarly, the optical O abundance is measured only from the O I 7777 Å triplet (Vennes et al. 2010; Melis et al. 2011). However, our abundance measurements for Si use many lines in the ultraviolet. In the recent compilation by Bautista et al. (2009) the authors combined several different computational methods, previous theoretical calculations by other authors and experimental data into a 'recommended' value for log *gf*. These values agree fairly well with the ultraviolet data from NIST that we have used. However, for the five optical lines they consider, the values are 0.25–0.30 dex smaller, though with errors as large as 0.3 dex. Using these values would *increase* the abundance determined from optical spectra, contrary to what would be needed for a more consistent solution. In addition, in a recent analysis of ultraviolet spectra for the DBZ star GD 40, Jura et al. (2012) find a discrepancy between optical and ultraviolet abundances for Si of the same size, but in opposite direction – the abundances are smaller for the optical determinations. Since that study used the same models and atomic data as the one presented here, there is no indication that the atomic data are behind this discrepancy.

Abundance stratification. Contrary to DB stars like GD 40 at similar temperatures, there are no convection zones in the atmospheres and envelopes of our four objects, which would act as a homogeneously mixed reservoir in the accretion/diffusion scenario. Assuming a steady state between the two processes, we thus expect a stratified abundance configuration. Whether this can explain the observations will be studied in Section 3.2.3.

Genuine variation of the accretion rates. As will also be discussed in the next section, the time-scales for diffusion in these atmospheres are of the order of days. If the accretion rate is not constant the observed abundances may change on the same short time-scales. Given that the COS and ground-based observations that we analysed were taken months to years apart, such variations cannot be excluded. Noticeable variations of the Ca II equivalent widths in the debris disc white dwarf G29-38 were reported by von Hippel & Thompson (2007). However, a similar study on the same star by Debes & López-Morales (2008) did not find any variations in the line strengths. Thus, the current evidence for accretion rate variations on time-scales of months to years is ambiguous, and a second-epoch COS observations of the stars studied here would be desirable.

We also noticed an unidentified absorption feature between 1400 and 1410 Å, with a strength roughly correlated with the Si

abundances. Such a feature has been discussed in the literature and related to an autoionization line of Si II or to a resonance feature in the photoionization cross-section (Artru & Lanz 1987; Lanz et al. 1996). We have tested such a hypothetical line with their data for the oscillator strength and line width data. However, the width (≈80 Å) is much too broad to lead to visible features in the spectrum. We have also included the Si II photoionization cross-sections from the Opacity Project (Seaton et al. 1994), which indeed show a resonance maximum in this spectral region. But again, the Si abundance is too small to let this feature show up in the spectrum.

Our model uses the six Si II lines at 1403.8, 1404.2, 1404.5, 1409.1, 1409.9 and 1410.2 Å in this range (Table 2). The first two have the source 'guess' in VALD, the first three have no entry in NIST, and the $\log gf$ values of the strongest line (1410.2 Å) differ by ≈0.8 dex between the two data bases. The upper levels of the transitions have a parent configuration belonging to the second ionization limit of Si II. They are still ≈0.7 eV below the first ionization limit and thus not strictly auto-ionizing. However, the broadening may well be underestimated by our simple approximation formulae. In summary, the atomic data of the lines in the region are very uncertain and may be the explanation for the broad feature. However, with the present data we cannot prove that hypothesis.

Finally, we note that the Si IV 1394, 1403 Å doublet in PG 0843+516 is very poorly fit by our atmosphere model (Fig. 3). A weaker additional Si IV 1394, 1403 Å absorption is also seen in the spectrum of SDSS 1228+1040 (Fig. 4). We interpret this as evidence for absorption by hot gas close to the white dwarf (see the discussion in Section 7).

3.2.3 *Diffusion and stratified atmosphere models*

In the absence of a convection zone there is no deep homogenous reservoir in our DAZ sample, and therefore there is no straightforward definition of diffusion time-scales. Adopting the usual definition, i.e. dividing the mass of some element above a layer in the envelope or atmosphere of the star by the diffusion flux, results in diffusion time-scales that strongly depend on the chosen layer. Koester & Wilken (2006) and Koester (2009) defined the Rosseland optical depth $\tau = 5$ as the 'standard' layer, assuming that no trace of any heavy element below this would be seen in a spectrum.

However, a more consistent way to determine the abundances in the accreted material, which is the quantity ultimately desired, is the assumption of a steady state between accretion and diffusion throughout the whole atmosphere. At Rosseland optical depth $\tau = 2/3$, and typical conditions for the observed ultraviolet spectra, the diffusion times in the four white dwarfs analysed here are ≃0.4 to 4 days. Assuming that the accretion rate does not vary over such time-scales, we can use the condition of constant flow of an element with mass fraction $X(\tau)$

$$\rho X v = \text{const}, \quad (1)$$

with ρ and v the mass density and the diffusion velocity of this element. ρ and v are known from the atmosphere model and diffusion calculations, and $X(\tau = 2/3)$ is derived from the spectral analysis. This determines the diffusion flux at $\tau = 2/3$. In steady state, as it is the case for the DAZ analysed here, the diffusion flux is constant throughout the atmosphere, and is equal to the accretion rate polluting the atmosphere. The constant diffusion flux then in turn allows the determination of the abundance stratification $X(\tau)$ (see also Vennes et al. 2011b, for a thorough discussion).

We calculated new stratified models and synthetic spectra for all objects, using the steady-state condition and the abundances (at $\tau = 2/3$) from Table 3. The resulting spectra are almost indistinguishable from those of the homogeneous atmospheres; the only exception are small increases of the optical Mg II and Ca II line strengths. The small change can easily be explained by the structure of the stratified atmosphere. In these models ρv increases with depth, and consequently the abundance decreases. On the other hand, a monochromatic optical depth of ≈2/3 is reached in the ultraviolet near Rosseland optical depth of $\tau_{\rm Ross} \simeq 2/3$, while it is reached at $\tau_{\rm Ross} \approx 0.15$ for $\lambda = 4480$ Å, i.e. higher in the atmosphere, where the abundance is correspondingly higher.

For PG 0843+516, PG 1015+161 and SDSS 1228+1040, the Ca and Mg abundances were obtained from the optical data (Section 2.2) and our models. We have iterated them by fitting to stratified models (denoted with 'strat' in Table 3). For GALEX 1931+0117, we adopted the photospheric Mg and Ca abundances of Vennes et al. (2011b) and the Mn abundance of Melis et al. (2011) to calculate the corresponding diffusion fluxes.

As a result we have to conclude that diffusion and a stratified abundance structure lead only to minor adjustments of the abundances that cannot explain the large discrepancy between optical and ultraviolet determinations for silicon. There is, however, an important caveat to this conclusion. Our diffusion calculations use only the surface gravity (and as a minor effect the temperature gradient for thermal diffusion) as driving force. Chayer & Dupuis (2010) have recently demonstrated that for silicon, radiative levitation can lead to a negative effective gravity and support the atoms in the outer layers of the atmosphere against diffusion. They only published detailed data for a DAZ model with 20 000 K and $\log g = 8.00$, and in their model only abundances smaller than $\log [{\rm Si/H}] = -8.0$ are really supported, because the lines saturate at higher abundances, effectively reducing the radiative support. However, it is quite feasible that even if the atoms are not totally supported, the diffusion velocity would be smaller, changing the abundance gradient. The answer to this puzzle will have to await similar, detailed models for a variety of stellar parameters and heavy elements that can be tested against the large range of Si abundances found in our snapshot survey (Gänsicke et al., in preparation).

Other points worth mentioning are that the determination of an effective ion charge with the simple pressure ionization description of Paquette et al. (1986) is not appropriate in the absence of deep convection. We have used the usual Saha equation (with a small lowering of the ionization potential from non-ideal interactions) to determine the abundances of different ions from an element. The diffusion velocity is then calculated as a weighted average of the ionization stages. This procedure was already used in Koester & Wilken (2006) and Koester (2009) for the models without or with only a shallow convection zone, although not explicitly stated in those papers. New in our present calculation is the consideration of neutral particles, following the discussion and methods outlined in Vennes, Kawka & Németh (2011a).

The main results of our calculations are the diffusion fluxes, $X\rho v$, for each element, which are assumed (in steady state) to be the abundances of the accreted matter. These are summarized for the four objects in Table 4. The total diffusion fluxes (= accretion rates) are obtained by multiplying these fluxes with $4\pi R^2_{\rm wd}$, where we used the cooling tracks of Wood (1995) to obtain the white dwarf radii from $T_{\rm eff}$ and $\log g$. The mass fluxes (= accretion rates) of the individual elements, as well as their sum, are shown in Fig. 5 and discussed in Section 6. The number abundances of the circumstellar

Table 4. Diffusion fluxes $\rho X v$ [g s^{-1}] within the white dwarf atmospheres, which are equal to the rates at which planetary debris material is accreted. Σ gives the sum of the accretions rates of all detected elements (i.e. not including those with upper limits). For GALEX 1931+0117, we adopt in our calculation the Mg and Ca abundances of Vennes et al. (2011b) and the Mn abundance of Melis et al. (2011) .

Element	PG 0843+516	PG 1015+161	SDSS 1228+1040	GALEX 1931+0117
C	1.66×10^5	4.65×10^4	1.25×10^5	4.57×10^5
O	9.27×10^7	3.78×10^7	2.70×10^8	5.61×10^8
Mg	4.47×10^7	2.66×10^7	3.21×10^7	1.47×10^8
Al	2.09×10^6		1.18×10^7	3.08×10^6
Si	4.77×10^7	3.64×10^6	4.80×10^7	9.93×10^7
P	2.44×10^6		$<5.24 \times 10^5$	7.57×10^5
S	3.92×10^7		$<9.46 \times 10^6$	2.64×10^6
Ca		4.84×10^6	1.57×10^7	8.10×10^6
Cr	3.81×10^7	$<3.85 \times 10^7$	$<2.29 \times 10^7$	1.37×10^7
Mn				1.06×10^7
Fe	7.11×10^8	9.50×10^7	1.72×10^8	6.45×10^8
Ni	1.66×10^7		$<9.98 \times 10^6$	4.71×10^6
Σ	1.02×10^9	1.68×10^8	5.61×10^8	1.50×10^9

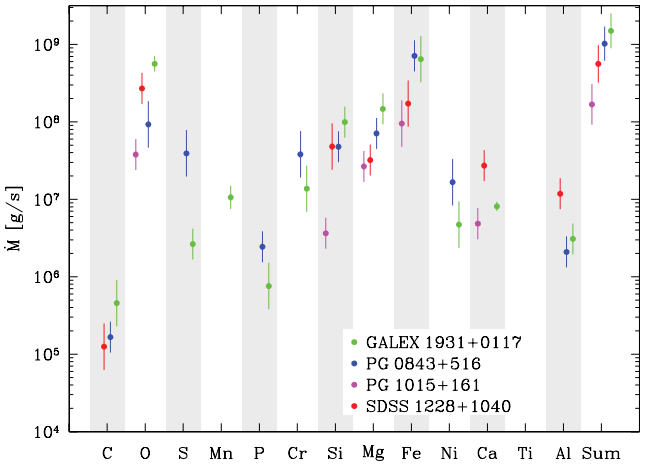

Figure 5. Accretion rates of the elements detected in our four targets. Their sum is given in the right-most column.

debris are then calculated from the diffusion fluxes via

$$\frac{N(\mathrm{X})}{N(\mathrm{Si})} = \frac{\dot{M}(\mathrm{X})}{\dot{M}(\mathrm{Si})} \frac{A(\mathrm{Si})}{A(\mathrm{X})} \qquad (2)$$

where A is the atomic mass. The implications that these abundances have on the nature and origin of the circumstellar debris are discussed in detail in Section 5.

4 NOTES ON INDIVIDUAL WHITE DWARFS

In the following sections, we give a brief overview of previous work on the four white dwarfs that we have analysed, as well as a summary of the key results of our observations.

4.1 PG 0843+516

PG 0843+516 was identified as a DA white dwarf in the Palomar–Green Survey (Green, Schmidt & Liebert 1986), and Liebert et al. (2005) obtained $T_{\rm eff} = 23\,870 \pm 392$ K, $\log g = 7.90 \pm 0.05$ from the analysis of a high-quality optical spectrum. The best fit to our *HST* data was $T_{\rm eff} = 23\,095 \pm 230$ K, $\log g = 8.17 \pm 0.06$. Our COS spectrum reveals PG 0843+516 to be an extremely polluted DAZ white dwarf (Figs 1 and 3), with an accretion rate of $\simeq 10^9$ g s^{-1}, placing it head-to-head with GALEX 1931+0117 (Section 6). We identified in the COS spectrum photospheric absorption lines of C, O, Al, Si, P, S, Fe, Cr and Ni, plus Mg in the optical WHT spectrum, the second largest set of elements detected in a DAZ white dwarf. The fact that the metal pollution of PG 0843+516 went unnoticed in the published high-quality intermediate-resolution spectroscopy underlines the strength of our ultraviolet survey for young and relatively warm white dwarfs accreting planetary debris. We note that Xu & Jura (2012) recently detected infrared flux excess at PG 0843+516 in an analysis of archival *Spitzer* data, making this the second white dwarf (after G29-38; Zuckerman & Becklin 1987; Koester, Provencal & Shipman 1997) where circumstellar dust was found without prior knowledge of photospheric metal pollution.

4.2 PG 1015+161

PG 1015+161 is another DA white dwarf discovered in the Palomar–Green Survey (Green et al. 1986). Liebert et al. (2005) determined $T_{\rm eff} = 19\,540 \pm 305$ K, $\log g = 8.04 \pm 0.05$ from optical spectroscopy. High-resolution spectroscopy of PG 1015+161 was obtained as part of the SPY project (Napiwotzki et al. 2001), from which Koester et al. (2009) measured $T_{\rm eff} = 19\,948 \pm 33$ K and $\log g = 7.925 \pm 0.006$. Our fit to the *HST* spectrum gives $T_{\rm eff} = 19\,200 \pm 180$ K, $\log g = 8.22 \pm 0.06$. Koester et al. (2005) detected of a photospheric Ca II K absorption line in the SPY data, with a number abundance $\log [\mathrm{Ca/H}] = -6.3$, which triggered follow-up observations with *Spitzer* that revealed the presence of circumstellar dust (Jura, Farihi & Zuckerman 2007). The COS spectrum contains absorption lines of O, Si and Fe. In addition to Ca II K, we detected Mg II 4482 Å in the SPY spectrum. PG 1015+161 has the lowest accretion rate among the four stars discussed in this paper.

4.3 SDSS 1228+1040

Eisenstein et al. (2006) identified this DA white dwarf in Data Release 4 of the Sloan Digital Sky Survey, and found $T_{\rm eff} = 22\,125 \pm 136$ K, $\log g = 8.22 \pm 0.02$ from a fit to the SDSS spectrum. Gänsicke et al. (2006) discovered double-peaked emission lines of Ca II 8498, 8542, 8662 Å as well as weak Fe II emission lines and Mg II 4482 Å absorption, and concluded that SDSS 1228+1040

accretes from a volatile-depleted gaseous circumstellar disc. The Ca II lines form in a region extending in radius from a few tenths $R_\odot$ to $\simeq 1.2\,R_\odot$, no emission is detected from closer in to the white dwarf (but see Section 7). *Spitzer* observations showed that SDSS 1228+1040 also exhibits an infrared excess (Brinkworth et al. 2009), and that there is a large radial overlap between the gaseous and dusty components of the disc. Yet, the strong Ca II emission lines require a gas temperature of $T \sim 4000$–6000 K (e.g. Hartmann et al. 2011), substantially exceeding the sublimation temperature of the dust. This implies the thermal decoupling of the gas and dust, most likely in the form of a complex vertical temperature structure, with hotter, optically thin gas on top cooler, probably optically thick dust (Melis et al. 2010; Kinnear 2011). Irradiation from the white dwarf is sufficient to explain this temperature inversion (Melis et al. 2010; Kinnear 2011), but the origin of the gas found at radii larger than the sublimation radius is unclear, and may be related to relatively fresh disruption events (Gänsicke et al. 2008; Melis et al. 2010) or the intrinsic evolution of the debris disc (Bochkarev & Rafikov 2011; Metzger et al. 2012). Among the four white dwarfs studied here, SDSS 1228+1040 is the only one that exhibits emission lines from a gaseous disc.

The COS spectrum of SDSS 1228+1040 contains absorption lines of C, O, Al, Si, Cr and Ni. SDSS 1228+1040 was observed outside the snapshot programme described in Section 2.1, and our COS spectroscopy extends up to 1790 Å, i.e. 360 Å further than that obtained for the other three white dwarfs. This extended wavelength range includes additional strong lines of Si II, Al II and Al III, but no further elements. Our high-quality average UVES spectrum is used to determine the abundances of Mg and Ca, bringing the total number of detected elements in SDSS 1228+1040 to eight.

We fitted the SDSS spectrum, finding $T_{\rm eff} = 22\,410 \pm 175$ K, $\log g = 8.12 \pm 0.03$, whereas a fit to the ultraviolet spectrum gives $T_{\rm eff} = 20\,565 \pm 82$ K, $\log g = 8.19 \pm 0.03$. This discrepancy underlines that, for high-quality data, the uncertainties are dominated by systematic rather than statistical errors. As a compromise we take the weighted mean of the latter two results with increased errors, $T_{\rm eff} = 20\,900 \pm 900$ K, $\log g = 8.15 \pm 0.04$.

4.4 GALEX 1931+0117

As part of a spectroscopic identification program of ultraviolet-excess objects Vennes et al. (2010) recently identified GALEX 1931+0117 as a nearby ($\simeq$55 pc) DAZ white dwarf. Vennes et al. (2010) and Melis et al. (2011) analysed optical spectroscopy, and obtained $T_{\rm eff} = 20\,890 \pm 120$ K, $\log g = 7.90^{+0.03}_{-0.06}$ and $T_{\rm eff} = 23\,470 \pm 300$ K, $\log g = 7.99 \pm 0.05$, respectively. Our best-fitting parameters from the *HST*/COS spectrum are $T_{\rm eff} = 21\,200 \pm 50$ K, $\log g = 7.91 \pm 0.02$, consistent with that of Vennes et al. (2010) but somewhat lower than that of Melis et al. (2011).[1] The VLT/UVES spectroscopy obtained by Vennes et al. (2010, 2011b) revealed strong metal lines of O, Mg, Si, Ca and Fe, indicating ongoing accretion. Vennes et al. (2010) also showed that the 2MASS *H*- and *K*-band fluxes exceeded those expected from the white dwarf, and suggested a close brown dwarf or a dusty debris disc as the origin of the accreting material. Debes et al. (2011) ruled out the presence of a sub-stellar companion based on the infrared fluxes detected by the Wide-Field Infrared Survey Explorer (WISE), and argued that the white dwarf accretes from a dusty disc. This was independently confirmed by obtained by Melis et al. (2011) using the Infrared Spectrometer and Array Camera (ISAAC) on the VLT, who also measured abundances for Cr and Mn.

Our *HST*/COS spectroscopy provides independent measurements for O, Si, Cr and Fe, as well as the first detection of C, Al, P, S and Ni, bringing the total number of elements observed in the photosphere of GALEX 1931+0117 to 11 (Table 3). As discussed in Section 3.2, the O, Si, Cr and Fe abundances that we derive from the COS spectroscopy are lower than those determined by Vennes et al. (2011b) and Melis et al. (2011). However, the discussion of the nature of the planetary material is usually based on relative metal-to-metal abundance ratios (Nittler et al. 2004), which are more robust than absolute abundances measurements. Fig. 6 compares the metal abundances determined for GALEX 1931+0117 normalized with respect to Si, and relative to the corresponding ratios for the chemical composition of the bulk Earth. It is evident that our metal-to-Si ratios are consistent with those of Melis et al. (2011), whereas the Mg/Si, Fe/Si and Ca/Si ratios of Vennes et al. (2011b) are systematically lower.

5 THE NATURE AND ORIGIN OF THE CIRCUMSTELLAR MATERIAL

The four white dwarfs studied here have diffusion time-scales of a few days (Section 3.2.3), and we can therefore safely assume that we observe them in accretion–diffusion equilibrium. In other words, the abundances of the circumstellar debris can be determined from the photospheric analysis without any additional assumptions regarding the history of the accretion rate that are necessary for stars with very long diffusion time-scales (e.g. Klein et al. 2011). In what follows, we discuss the abundances of the circumstellar debris normalized to Si, the main rock-forming element, as is common use for Solar system objects (e.g. Lodders & Fegley 2011).

Fig. 6 (right-hand panel) illustrates the metal-to-Si ratios of the planetary debris around the four white dwarfs relative to the same abundances of the bulk Earth model by McDonough (2000). The first striking observation is that the C/Si ratios of all four stars (including one upper limit) are much lower than that of CI chondrites, and in fact agree within their errors with the C/Si value of the bulk Earth model. While the C abundance of the bulk Earth is subject to some model-dependent assumptions (see the left-hand panel of Fig. 6 for an alternative chemical model of the Earth by Allègre, Manhès & Lewin 2001), these uncertainties are comparable to the errors in our abundance determinations.

For comparison, we include in Fig. 6 the abundance ratios of three white dwarfs that accrete from the wind of a close M-dwarf companion, that were also observed as part of our COS snapshot programme.[2] The only elements detected in the COS spectra of these three stars are C, O, Si and S, and they exhibit high abundances in C and S, as expected for the accretion of solar-like material. The extremely low abundances of the volatile C found for the debris around the four white dwarfs strongly underline its rocky nature. This corroborates the previous studies of Jura (2006) and Jura et al.

[1] Melis et al. (2011) discuss the discrepancy between their model and the *GALEX* fluxes. From their table 1, it appears that they did not correct for the non-linearity of the *GALEX* detectors for bright targets. The corrected *GALEX* magnitudes given by Vennes et al. (2010) are in good agreement with our best-fitting model.

[2] A more detailed discussion of these binaries will be published elsewhere. Here, they merely serve as 'abundance standard white dwarfs' which accrete material with abundance ratios that are expected to be close to solar, i.e. rich in volatiles.

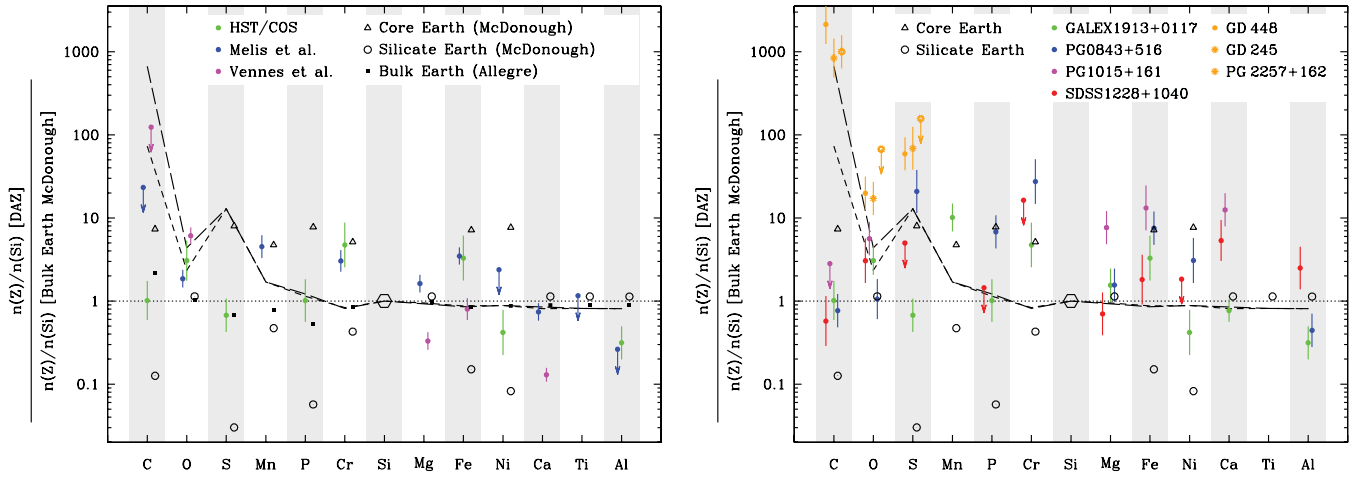

Figure 6. Heavy element abundances derived for the circumstellar debris at the four white dwarf targets (see Table 4), relative to Si, and normalized to the same ratios of the bulk Earth (McDonough 2000). The elements are arranged, left to right, in order of increasing sublimation temperature (Lodders 2003). Left-hand panel: abundances for the debris around GALEX 1931+0117 (green: this paper, blue: Melis et al. 2011, magenta: Vennes et al. 2011b). Also shown are the abundance ratios for the core Earth (which makes up ∼1/3 of the Earth's mass, open triangles) and the silicate Earth (i.e. crust and mantle, which make up ∼2/3 of the Earth's mass, open circles). The bulk Earth composition of Allègre et al. (1995) is shown as solid black squares, illustrating the level of uncertainty in the (model-dependent) composition of the Earth. The short-dashed line shows the abundance ratios of CI chondrites, and the long-dashed line those corresponding to solar abundances (both from Lodders 2003). Right-hand panel: metal-to-Si ratios for PG 0843+516 (blue), PG 1015+161 (magenta), SDSS 1228+1040 (red) and GALEX 1931+0117 (green). Shown in orange are the abundance ratios of three white dwarfs that accrete from the wind of a close M-dwarf companion. As expected for the accretion of material with near-solar abundances, the volatiles C and S are found to be strongly enhanced compared to the four white dwarfs that host debris discs of exo-terrestrial material.

(2012), who found strong evidence for substantial depletion of C around three DB white dwarfs.

However, Fig. 6 also shows that there is a significant scatter among the individual abundances for a given element. Among the four targets, the abundances of the debris in SDSS 1228+1040 most closely resemble those of the bulk Earth. PG 1015+161 stands out by having all detected elements overabundant with respect to Si, when compared to the bulk Earth. An interesting trend is seen in PG 0843+516, where Fe, Ni and S are significantly overabundant, and, in fact, broadly consistent with the abundance ratios of the core Earth model. In particular, the volatile S is extremely overabundant with respect to C, compared to the bulk silicate Earth. In melts, S will form FeS, and hence be depleted from remaining minerals. The affinity of S to Fe is thought to be the reason for the depletion of S in the silicate mantle of the Earth, as it will have settled into the Earth's core in the form of iron sulphide (Ahrens 1979; Dreibus & Palme 1996). Similarly, also Cr is significantly overabundant in PG 0843+516 with respect to the bulk Earth. While Cr is a moderately volatile element, the depletion of Cr in the silicate Earth is thought to be due to partitioning into the Earth's core (Moynier, Yin & Schauble 2011). Finally, the refractory lithophile Al is underabundant compared to the silicate Earth. Thus, the abundance pattern seen in PG 0843+516 suggests that the planetary debris is rich in material that has undergone at least partial melting, and possibly differentiation. A possible test of this hypothesis would be a measurement of the abundance of Zn, a lithophile element with a similar volatility as S that is not depleted into iron melt (Lodders 2003), and it will be important to test whether the refractory lithophile Ca is depleted at a similar level as Al. The most promising feature to measure the Zn abundances is the Zn II 2026, 2062 Å resonance doublet, and Ca II K should be easily detectable in high-resolution optical spectroscopy.

To further explore the chemical diversity of the planetary debris around the four white dwarfs studied here, we compare pairwise a range of metal-to-Si abundance ratios with those of the bulk Earth and bulk silicate Earth (McDonough 2000), as well as with those of a variety of meteorites (taken from Nittler et al. 2004). We inspect first the relative abundances of Al and Ca, which are two of the three most abundant refractory lithophile elements (the third one being Ti), i.e. elements that sublimate only at very high temperatures, and that do not enter the core in the case of differentiation. Therefore, the Al/Ca ratio is nearly constant across most classes of meteorites, and, hence, the Al/Si values determined from many Solar system bodies follow a linear correlation with Ca/Si (Fig. 7, top right). Finding that the abundances for the debris discs, where Al, Ca and Si are available, generally follow that trend is reassuring, as large variations in the relative Al and Ca abundances would cast doubts on the overall methodology using white dwarf photospheres as proxies for the abundances of the circumstellar material.

The relative abundances of O, Si, Mg and Fe, which are the major constituents of the terrestrial planets in the Solar system, show substantial variations between different meteorite groups (Fig. 7, top-left and bottom-right panels), and at least as much scatter between the individual white dwarfs. The difficulty with these elements is that they form a range of different minerals (metal oxides), depending on the prevailing pressure and temperature. Iron in particular may occur as pure metal, alloy or mineral, and is subject to differentiation into planetary cores. Oxygen, on the other hand, can be locked in a wide range of oxides (see the discussion by Klein et al. 2010), or potentially water (Jura & Xu 2010, 2012; Klein et al. 2010; Farihi et al. 2011). Therefore, the relative abundances of O, Si, Mg and Fe will vary according to the processing that material underwent (e.g. condensation, melting and differentiation), and it is, maybe, not too surprising to find that the debris around white dwarfs exhibits at substantial degree of diversity, as it represents different planetary systems formed around different stars. We note that the debris at PG 0843+516 falls close to the abundance ratios of pallasites, a class of stony-iron meteorites. This further supports

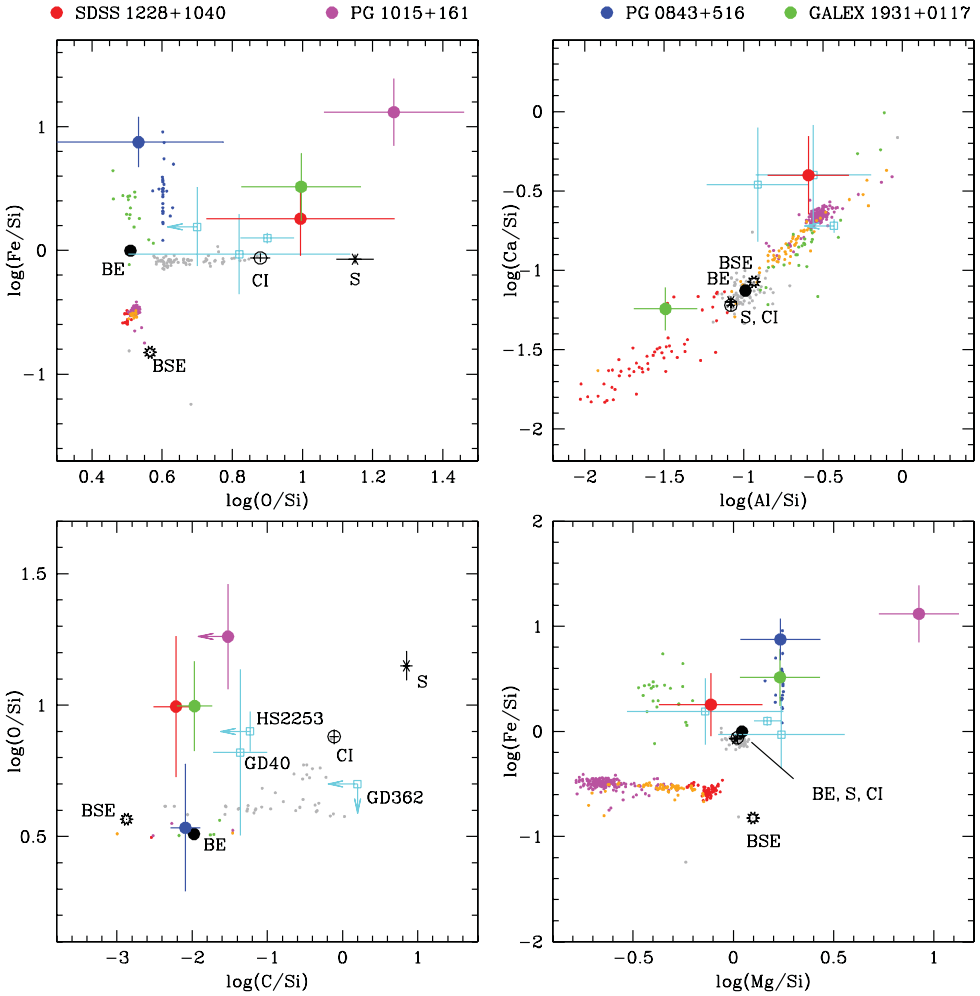

Figure 7. The chemical abundances of planetary debris, determined from the photospheric studies of polluted white dwarfs, reveal a large degree of diversity. The four panels illustrate a range of metal-to-Si number abundance ratios for the four stars analysed in this paper, compared to those of bulk Earth and bulk silicate Earth (BE and BSE; McDonough 2000), solar abundances and CI chondrites (S and CI; Lodders 2003), and several meteorite classes (grey = carbonaceous chondrites, green = mesoderites, blue = pallasites, red = diogenites, orange = howardites, magenta = eucrites; Nittler et al. 2004). Also shown, in light blue, are the abundance ratios for the polluted DB white dwarfs GD 362 (Zuckerman et al. 2007), GD 40 (Jura et al. 2012) and HS 2253+8023 (Klein et al. 2011).

our hypothesis that PG 0843+516 is accreting material in which iron has undergone (partial) melting.

Another interesting pair of elements is C and O (Fig. 7, lower-left panel). The possible range of the C/O ratio among exo-planets has been subject to intense discussion. It is thought that for C/O > 0.8 in the protoplanetary discs, the ambient chemistry will favour solid 'carbon planets', which are dominated by carbides rather than oxides (Kuchner & Seager 2005). The possible existence of carbon planets has gained some support by the recent report of a C/O value exceeding unity in the atmosphere of the transiting hot Jupiter WASP-12b (Madhusudhan et al. 2011), and by abundance studies that found a significant fraction of exo-planet host stars having C/O > 0.8 (Delgado Mena et al. 2010; Petigura & Marcy 2011), but see Fortney (2012) for a critical discussion.

Planetary debris at white dwarfs provides a unique opportunity to probe the C/O ratio of exo-terrestrial material. However, measuring C abundances in white dwarfs is challenging, as the optical detection of carbon in cool white dwarfs is usually related to dredge-up from the core rather than external pollution (e.g. Dufour, Bergeron & Fontaine 2005; Koester & Knist 2006; Desharnais et al. 2008). At higher temperatures, where convective dredge-up can be excluded, suitable lines of C are only found at ultraviolet wavelengths. As mentioned above, the four stars studied here have very similar (low) C/Si ratios, but do show a range of O/Si ratios. Nevertheless, the debris around all four stars studied here, as well as GD 40 (Jura et al. 2012), have $-3 \lesssim \log(\mathrm{C/O}) \lesssim -2.3$, very similar to the bulk silicate Earth, $\log(\mathrm{C/O}) \simeq -2.5$, and are hence representative of Solar system minerals.

6 ACCRETION RATES

Estimating accretion rates for metal-polluted white dwarfs is notoriously difficult as it is based on scaling from the elements detected in the photosphere to an assumed bulk composition of the accreted material. In addition, in the case of white dwarfs with significant convective envelope masses, only the average accretion rate over the diffusion time-scale can be obtained.

Koester & Wilken (2006) calculated accretion rates for 38 DAZ white dwarfs based on the abundance of Ca, and adopting solar abundances for the accreting material. For PG 1015+161, these

assumptions implied $\dot{M} \simeq 2 \times 10^{11}\,\mathrm{g\,s^{-1}}$. Since then, it has become increasingly clear that many, if not most, metal-polluted (single) white dwarfs accrete volatile-depleted material from circumstellar planetary debris. Farihi et al. (2009) estimated accretion rates for 53 metal-polluted white dwarfs following the prescription of Koester & Wilken (2006), but scaling the results by the typical gas-to-dust ratio in the interstellar medium to account for the absence of H and He in the accreted debris, resulting in $\dot{M} \simeq 2 \times 10^{9}\,\mathrm{g\,s^{-1}}$ for PG 1015+161.

The uncertainty in the estimated accretion rates can be greatly reduced if photospheric abundances for the major constituents of the debris material can be measured. While we do not detect all elements that are likely present in the circumstellar debris at the four white dwarfs studied here, we have determined the accretion rates of all the major elements, in particular O, Si, Mg and Fe (Section 3.2.3). The accretion rates of all detected elements, as well as their sum, are given in Table 4, and are illustrated in Fig. 5. For PG 1015+161, we find $\dot{M} \simeq 1.7 \times 10^{8}\,\mathrm{g\,s^{-1}}$, which is strictly speaking a lower limit; however, the undetected elements (e.g. Al, S, Ti, Mn, Cr) are unlikely to contribute more than 10 per cent of the total accretion rate. Similarly, we find the accretion rates of PG 0843+516, SDSS 1228+1040 and GALEX 1931+0117 to be $\dot{M} \simeq 1.0 \times 10^{9}\,\mathrm{g\,s^{-1}}$, $5.6 \times 10^{8}\,\mathrm{g\,s^{-1}}$ and $1.5 \times 10^{9}\,\mathrm{g\,s^{-1}}$, respectively.

7 HOT CIRCUMSTELLAR GAS

The discs around white dwarfs are passive, i.e. their emission is solely due to the thermal reprocessing of intercepted stellar flux. The inner disc radius where typical dust grains will rapidly sublimate is determined by the luminosity of the white dwarf (von Hippel et al. 2007). The gaseous material will viscously spread, both flowing inwards on to the white dwarf and outwards over the dusty disc, potentially accelerating the inwards migration of the dust via aerodynamic drag (Rafikov 2011). While gaseous material orbiting at radii coincident with circumstellar dust is observed in a number of systems in the form of double-peaked emission lines (Gänsicke et al. 2006, 2007, 2008; Brinkworth et al. 2009, 2012; Melis et al. 2011, 2012; Dufour et al. 2012; Farihi et al. 2012b), there has, as yet, been no detection of gaseous material well inside the sublimation radius.

Inspection of Fig. 3 reveals that the strength of the Si IV 1394, 1403 Å doublet in PG 0843+516 is extremely underpredicted by the photospheric model. These Si IV lines correspond to the highest ionization energy of all transitions detected in the COS spectrum. For the temperature and the Si abundance of PG 0843+516, the observed strength of the Si IV lines is absolutely incompatible with a purely photospheric origin. The most plausible explanation is that there is additional absorption along the line of sight, associated with hot gas close to the white dwarf that is optically thin except for the strong resonance lines of high-ionization species, such as Si IV. In fact, extremely similar features were found in the far-ultraviolet observations of cataclysmic variables, i.e. white dwarfs that accrete from an (hydrogen-rich) accretion disc that is in turn fed by Roche lobe overflow of a close M-dwarf companion. *HST*/GHRS (Goddard High Resolution Spectrograph) and *FUSE* (Far Ultraviolet Spectrograph Explorer) spectroscopy of the white dwarf in U Gem contain very strong absorption of N V 1239, 1243 Å and O VI 1032, 1038 Å that cannot form in the ≃30 000 K photosphere, as well as excess absorption in Si II 1394, 1403 Å (Sion et al. 1998; Long & Gilliland 1999; Long, Brammer & Froning 2006). All three high-ionization doublets are redshifted with respect to the systemic velocity of the white dwarf, but somewhat less so than the lower-ionization photospheric lines, which are subject to the gravitational redshift at the photospheric radius. These observations were interpreted as evidence for a hot (∼80 000 K) layer of gas sufficiently close to the white dwarf to still experience a noticeable gravitational redshift. Measuring the central wavelengths of the strong Si IV 1394, 1403 Å lines in PG 0843+516, we find that they are blueshifted with respect to the photospheric features by $\simeq 25\,\mathrm{km\,s^{-1}}$, which implies a height of ≃1.5 white dwarf radii above the white dwarf surface. This assumes that there is no significant flow velocity, which seems reasonably well justified given the symmetric shape of the Si IV profiles.

A discrepancy between the best-fitting white dwarf model and the region around the Si IV doublet is also seen in the COS spectrum of SDSS 1228+1040 (Fig. 4, bottom-left panel); however, in this star, the additional absorption is rather weak. These additional absorption features are clearly blueshifted with respect to the photospheric lines; however, the relatively low S/N of the spectrum prevents an accurate determination of this offset.

For PG 1015+161 and GALEX 1931+0117, the photospheric fits match the observed Si IV lines well, i.e. there is no evidence for any additional absorption component. Given that these two stars have, respectively, the lowest and highest accretion rate of our small sample (Section 6), there seems to be no clear correlation between the detection of absorption from highly ionized gas to the mass flow rate on to the white dwarf. A key difference between the two stars where circumstellar Si IV absorption is detected is that SDSS 1228+1040 also shows strong *emission* lines from circumstellar gas, which indicate a relatively high inclination of the accretion disc. In contrast, no gaseous emission is found in PG 0843+516 (Gänsicke et al., in preparation). Identifying additional absorption features from these hot layers of gas would provide substantial constraints on the physical parameters in the corresponding regions. The strongest line seen in cataclysmic variables, N V, is naturally absent in the white dwarfs accreting rocky debris,[3] but the O VI 1032, 1038 Å doublet detected in U Gem (Long et al. 2006) is a promising candidate.

8 CONCLUSIONS

Recent years have seen a surge of interest in the evolution of extra-solar planetary systems through the late phases in the lives of their host stars (e.g. Burleigh, Clarke & Hodgkin 2002; Debes & Sigurdsson 2002; Villaver & Livio 2007, 2009; Di Stefano, Howell & Kawaler 2010; Nordhaus et al. 2010). While no planet has yet been discovered orbiting a white dwarf (Hogan, Burleigh & Clarke 2009; Faedi et al. 2011), significant progress has been made in the discovery and understanding of planetary debris discs around white dwarfs.

Our COS study substantially increases the number of polluted white dwarfs for which a wide range of chemical elements have been detected. We find that the C/Si ratio is consistent with that of the bulk Earth, which confirms the rocky nature of the debris at these white dwarfs, and their C/O values, are typical of

[3] For completeness, we note that circumstellar high-ionization absorption lines have also been found around a number of hot white dwarfs (Bannister et al. 2003; Dickinson et al. 2012). However, the origin of the circumstellar material is not clear, and the detection of strong C lines suggests a different nature compared to the rocky debris found around the stars studied here.

minerals dominated by Fe and Mg silicates. There is so far no detection of planetary debris at white dwarfs that has a large C/O ratio which would be indicative of silicon carbide-based minerals. The abundances of planetary material found around white dwarfs show a large diversity, comparable to, or exceeding, that seen among different meteorite classes in the Solar system. We find that the Al/Ca ratio follows a similar trend as observed among Solar system objects, which suggests that processing of proto- and post-planetary material follows similar underlying principles. A particularly interesting pattern is found in PG 0843+516, where overabundances of S, Cr, Fe and Ni are suggestive of the accretion of material that underwent melting and possibly differentiation. Extending the abundance studies of metal-polluted white dwarfs in both detail and number will provide further insight into the diversity of exo-terrestrial material, and guide the understanding of terrestrial exo-planet formation (Bond, O'Brien & Lauretta 2010; Carter-Bond et al. 2012).

ACKNOWLEDGMENTS

We gratefully acknowledge Larry Nittler for sharing his meteorite abundance data with us, and William Januszewski, Charles Proffitt and Elena Mason for their tireless efforts in the implementation of the *HST* programme. DK wants to thank P.-E. Tremblay and P. Bergeron for sharing their new calculations of the hydrogen Lyman and Balmer line Stark profiles. Based on observations made with the NASA/ESA *HST*, obtained at the Space Telescope Science Institute, which is operated by the Association of Universities for Research in Astronomy, Inc., under NASA contract NAS 5-26555. These observations are associated with program 11561, 12169 and 12474. Also based on observations made with ESO Telescopes at the La Silla Paranal Observatory under programme ID 79.C-0085, 81.C-0466, 82.C-0495 and 383.C-0695. We thank the anonymous referee for a constructive report.

REFERENCES

Aannestad P. A., Kenyon S. J., Hammond G. L., Sion E. M., 1993, AJ, 105, 1033
Ahrens T. J., 1979, J. Geophys. Res., 84, 985
Allègre C. J., Poirier J., Humler E., Hofmann A. W., 1995, Earth Planet. Sci. Lett., 134, 515
Allègre C., Manhès G., Lewin E., 2001, Earth Planet. Sci. Lett., 185, 49
Artru M.-C., Lanz T., 1987, A&A, 182, 273
Bannister N. P., Barstow M. A., Holberg J. B., Bruhweiler F. C., 2003, MNRAS, 341, 477
Bautista M. A., Quinet P., Palmeri P., Badnell N. R., Dunn J., Arav N., 2009, A&A, 508, 1527
Becklin E. E., Farihi J., Jura M., Song I., Weinberger A. J., Zuckerman B., 2005, ApJ, 632, L119
Bochkarev K. V., Rafikov R. R., 2011, ApJ, 741, 36
Bond J. C., O'Brien D. P., Lauretta D. S., 2010, ApJ, 715, 1050
Bonsor A., Mustill A. J., Wyatt M. C., 2011, MNRAS, 414, 930
Brinkworth C. S., Gänsicke B. T., Marsh T. R., Hoard D. W., Tappert C., 2009, ApJ, 696, 1402
Brinkworth C. S., Gänsicke B. T., Girven J. M., Hoard D. W., Marsh T. R., Parsons S. G., Koester D., 2012, ApJ, 750, 86
Burleigh M. R., Clarke F. J., Hodgkin S. T., 2002, MNRAS, 331, L41
Carter-Bond J. C., O'Brien D. P., Delgado Mena E., Israelian G., Santos N. C., González Hernández J. I., 2012, ApJ, 747, L2
Chayer P., Dupuis J., 2010, in Werner K., Rauch T., eds, AIP Conf. Ser. 1273, 17th European White Dwarf Workshop, Am. Inst. Phys., New York, p. 394
Chayer P., Fontaine G., Wesemael F., 1995, ApJS, 99, 189
Debes J. H., López-Morales M., 2008, ApJ, 677, L43
Debes J. H., Sigurdsson S., 2002, ApJ, 572, 556
Debes J. H., Hoard D. W., Kilic M., Wachter S., Leisawitz D. T., Cohen M., Kirkpatrick J. D., Griffith R. L., 2011, ApJ, 729, 4
Debes J. H., Walsh K. J., Stark C., 2012, ApJ, 747, 148
Delgado Mena E., Israelian G., González Hernández J. I., Bond J. C., Santos N. C., Udry S., Mayor M., 2010, ApJ, 725, 2349
Desharnais S., Wesemael F., Chayer P., Kruk J. W., Saffer R. A., 2008, ApJ, 672, 540
Dickinson N. J., Barstow M. A., Welsh B. Y., Burleigh M., Farihi J., Redfield S., Unglaub K., 2012, MNRAS, in press (arXiv:1203.5226)
Di Stefano R., Howell S. B., Kawaler S. D., 2010, ApJ, 712, 142
Dreibus G., Palme H., 1996, Geochimica et Cosmochimica Acta, 60, 1125
Dufour P., Bergeron P., Fontaine G., 2005, ApJ, 627, 404
Dufour P., Kilic M., Fontaine G., Bergeron P., Melis C., Bochanski J., 2012, ApJ, 749, 6
Dupuis J., Fontaine G., Wesemael F., 1993, ApJS, 87, 345
Eisenstein D. J. et al., 2006, ApJS, 167, 40
Faedi F., West R. G., Burleigh M. R., Goad M. R., Hebb L., 2011, MNRAS, 410, 899
Farihi J., Zuckerman B., Becklin E. E., 2008, ApJ, 674, 431
Farihi J., Jura M., Zuckerman B., 2009, ApJ, 694, 805
Farihi J., Barstow M. A., Redfield S., Dufour P., Hambly N. C., 2010a, MNRAS, 404, 2123
Farihi J., Hoard D. W., Wachter S., 2010b, ApJS, 190, 275
Farihi J., Brinkworth C. S., Gänsicke B. T., Marsh T. R., Girven J., Hoard D. W., Klein B., Koester D., 2011, ApJ, 728, L8
Farihi J., Gänsicke B. T., Wyatt M. A., Girven J., Pringle J. E., King A. R., 2012a, MNRAS, in press (arXiv:1205.0004)
Farihi J., Gänsicke B. T., Steele P. R., Girven J., Burleigh M. R., Breedt E., Koester D., 2012b, MNRAS, 421, 1635
Fontaine G., Michaud G., 1979, ApJ, 231, 826
Fontaine G., Villeneuve B., Wesemael F., Wegner G., 1984, ApJ, 277, L61
Fortney J. J., 2012, ApJ, 747, L27
Friedrich S., Jordan S., Koester D., 2004, A&A, 424, 665
Gänsicke B. T., Marsh T. R., Southworth J., Rebassa-Mansergas A., 2006, Sci, 314, 1908
Gänsicke B. T., Marsh T. R., Southworth J., 2007, MNRAS, 380, L35
Gänsicke B. T., Koester D., Marsh T. R., Rebassa-Mansergas A., Southworth J., 2008, MNRAS, 391, L103
Girven J., Brinkworth C. S., Farihi J., Gänsicke B. T., Hoard D. W., Marsh T. R., Koester D., 2012, ApJ, 749, 154
Graham J. R., Matthews K., Neugebauer G., Soifer B. T., 1990, ApJ, 357, 216
Green R. F., Schmidt M., Liebert J., 1986, ApJS, 61, 305
Grillmair C. J. et al., 2008, Nat, 456, 767
Hartmann S., Nagel T., Rauch T., Werner K., 2011, A&A, 530, A7
Hogan E., Burleigh M. R., Clarke F. J., 2009, MNRAS, 396, 2074
Jura M., 2003, ApJ, 584, L91
Jura M., 2006, ApJ, 653, 613
Jura M., Xu S., 2010, AJ, 140, 1129
Jura M., Xu S., 2012, AJ, 143, 6
Jura M., Farihi J., Zuckerman B., 2007, ApJ, 663, 1285
Jura M., Xu S., Klein B., Koester D., Zuckerman B., 2012, ApJ, 750, 69
Kilic M., von Hippel T., Leggett S. K., Winget D. E., 2005, ApJ, 632, L115
Kinnear T., 2011, Master's thesis, Univ. Warwick
Klein B., Jura M., Koester D., Zuckerman B., Melis C., 2010, ApJ, 709, 950
Klein B., Jura M., Koester D., Zuckerman B., 2011, ApJ, 741, 64
Koester D., 1976, A&A, 52, 415
Koester D., 2009, A&A, 498, 517
Koester D., 2010, Memor. Soc. Astronom. Ital., 81, 921
Koester D., Knist S., 2006, A&A, 454, 951
Koester D., Wilken D., 2006, A&A, 453, 1051
Koester D., Weidemann V., Zeidler E.-M., 1982, A&A, 116, 147
Koester D., Provencal J., Shipman H. L., 1997, A&A, 320, L57
Koester D., Rollenhagen K., Napiwotzki R., Voss B., Christlieb N., Homeier D., Reimers D., 2005, A&A, 432, 1025

Koester D., Voss B., Napiwotzki R., Christlieb N., Homeier D., Lisker T., Reimers D., Heber U., 2009, A&A, 505, 441
Kuchner M. J., Seager S., 2005, ApJ, in press (arXiv:1201.6252)
Kupka F., Piskunov N., Ryabchikova T. A., Stempels H. C., Weiss W. W., 1999, A&AS, 138, 119
Kupka F. G., Ryabchikova T. A., Piskunov N. E., Stempels H. C., Weiss W. W., 2000, Baltic Astron., 9, 590
Lajoie C., Bergeron P., 2007, ApJ, 667, 1126
Lanz T., Artru M.-C., 1985, Phys. Scr., 32, 115
Lanz T., Barstow M. A., Hubeny I., Holberg J. B., 1996, ApJ, 473, 1089
Liebert J., Bergeron P., Holberg J. B., 2005, ApJS, 156, 47
Lodders K., 2003, ApJ, 591, 1220
Lodders K., Fegley B., 2011, Chemistry of the Solar System. RSC Publishing, Cambridge
Long K. S., Gilliland R. L., 1999, ApJ, 511, 916
Long K. S., Brammer G., Froning C. S., 2006, ApJ, 648, 541
McDonough W., 2000, in Teisseyre R., Majewski E., eds, Earthquake Thermodynamics and Phase Transformation in the Earth's Interior. Academic Press, San Diego, p. 5
Madhusudhan N. et al., 2011, Nat, 469, 64
Maxted P. F. L., Marsh T. R., Moran C., Dhillon V. S., Hilditch R. W., 1998, MNRAS, 300, 1225
Melis C., Jura M., Albert L., Klein B., Zuckerman B., 2010, ApJ, 722, 1078
Melis C., Farihi J., Dufour P., Zuckerman B., Burgasser A. J., Bergeron P., Bochanski J., Simcoe R., 2011, ApJ, 732, 90
Melis C. et al., 2012, ApJ, 751, L4
Metzger B. D., Rafikov R. R., Bochkarev K. V., 2012, MNRAS, in press (arXiv:1202.0557)
Moynier F., Yin Q.-Z., Schauble E., 2011, Sci, 331, 1417
Nahar S. N., 1998, Atomic Data Nuclear Data Tables, 68, 183
Napiwotzki R. et al., 2001, Astron. Nachr., 322, 411
Nittler L. R., McCoy T. J., Clark P. E., Murphy M. E., Trombka J. I., Jarosewich E., 2004, Antarctic Meteorite Res., 17, 231
Nordhaus J., Spiegel D. S., Ibgui L., Goodman J., Burrows A., 2010, MNRAS, 408, 631
Paquette C., Pelletier C., Fontaine G., Michaud G., 1986, ApJS, 61, 177
Petigura E. A., Marcy G. W., 2011, ApJ, 735, 41
Piskunov N. E., Kupka F., Ryabchikova T. A., Weiss W. W., Jeffery C. S., 1995, A&AS, 112, 525
Pyrzas S. et al., 2012, MNRAS, 419, 817
Rafikov R. R., 2011, MNRAS, 416, L55
Ryabchikova T. A., Piskunov N. E., Kupka F., Weiss W. W., 1997, Baltic Astron., 6, 244
Schmidt G. D., Smith P. S., Harvey D. A., Grauer A. D., 1995, AJ, 110, 398
Schreiber M. R., Gänsicke B. T., 2003, A&A, 406, 305
Seaton M. J., Yan Y., Mihalas D., Pradhan A. K., 1994, MNRAS, 266, 805
Sion E. M., Cheng F. H., Szkody P., Sparks W., Gänsicke B., Huang M., Mattei J., 1998, ApJ, 496, 449
Tremblay P.-E., Bergeron P., 2009, ApJ, 696, 1755
Valencia D., Ikoma M., Guillot T., Nettelmann N., 2010, A&A, 516, A20
van Maanen A., 1917, PASP, 29, 258
Vennes S., Kawka A., Németh P., 2010, MNRAS, 404, L40
Vennes S., Kawka A., Németh P., 2011a, in Schuh S., Drechsel H., Heber U., eds, AIP Conf. Ser. 1331, Planetary Systems beyond the Main Sequence. Am. Inst. Phys., New York, p. 246
Vennes S., Kawka A., Németh P., 2011b, MNRAS, 413, 2545
Villaver E., Livio M., 2007, ApJ, 661, 1192
Villaver E., Livio M., 2009, ApJ, 705, L81
von Hippel T., Thompson S. E., 2007, ApJ, 661, 477
von Hippel T., Kuchner M. J., Kilic M., Mullally F., Reach W. T., 2007, ApJ, 662, 544
Wachter S., Hoard D. W., Hansen K. H., Wilcox R. E., Taylor H. M., Finkelstein S. L., 2003, ApJ, 586, 1356
Wesemael F., 1979, A&A, 72, 104
Wood M. A., 1995, in Koester D., Werner K., eds, White Dwarfs, no. 443 in LNP. Springer, Heidelberg, p. 41
Xu S., Jura M., 2012, ApJ, 745, 88
Zuckerman B., Becklin E. E., 1987, Nat, 330, 138
Zuckerman B., Koester D., Melis C., Hansen B. M., Jura M., 2007, ApJ, 671, 872
Zuckerman B., Koester D., Dufour P., Melis C., Klein B., Jura M., 2011, ApJ, 739, 101

This paper has been typeset from a TEX/LATEX file prepared by the author.